ORIGINAL RESEARCH

iRGD-Guided Silica/Gold Nanoparticles for Efficient Tumor-Targeting and Enhancing Antitumor Efficacy Against Breast Cancer

Xuefeng Hou[1–4],*, Qi Chen[1],*, Ying Fang[5], Li Zhang[1], Shuoheng Huang[1], Minjie Xu[1], Yaning Ren[1], Zhansen Shi[1], Yan Wei[1], Lihua Li[1–4]

[1]School of Pharmacy, Wannan Medical College, Wuhu, Anhui Province, People's Republic of China; [2]Anhui Provincial Engineering Laboratory for Screening and Re-Evaluation of Active Compounds of Herbal Medicines in Southern Anhui, Wannan Medical College, Wuhu, Anhui Province, People's Republic of China; [3]Anhui Provincial Engineering Research Center for Polysaccharide Drugs, Wannan Medical College, Wuhu, Anhui Province, People's Republic of China; [4]Drug Research and Development Center, Wannan Medical College, Wuhu, Anhui Province, People's Republic of China; [5]School of Pharmacy, Shanghai University of Traditional Chinese Medicine, Shanghai, People's Republic of China

*These authors contributed equally to this work

Correspondence: Yan Wei; Lihua Li, School of Pharmacy, Wannan Medical College, No. 22, West Wenchang Road, Wuhu, 241002, People's Republic of China, Email yanwei@wnmc.edu.cn; llh05530226@126.com

Background: Breast cancer presents significant challenges due to the limited effectiveness of available treatments and the high likelihood of recurrence. iRGD possesses both RGD sequence and C-terminal sequence and has dual functions of targeting and membrane penetration. iRGD-modified nanocarriers can enhance drug targeting of tumor vascular endothelial cells and penetration of new microvessels, increasing drug concentration in tumor tissues.

Methods: The amidation reaction was carried out between $SiO_2/AuNCs$ and iRGD/PTX, yielding a conjugated drug delivery system ($SiO_2/AuNCs$-iRGD/PTX, SAIP@NPs). The assessment encompassed the characterization of the morphology, particle size distribution, physicochemical properties, in vitro release profile, cytotoxicity, and cellular uptake of SAIP@NPs. The tumor targeting and anti-tumor efficacy of SAIP@NPs were assessed using a small animal in vivo imaging system and a tumor-bearing nude mice model, respectively. The tumor targeting and anti-tumor efficacy of SAIP@NPs were assessed utilizing a small animal in vivo imaging system and an in situ nude mice breast cancer xenograft model, respectively.

Results: The prepared SAIP@NPs exhibited decent stability and a certain slow-release effect in phosphate buffer (PBS, pH 7.4). In vitro studies had shown that, due to the dual functions of transmembrane and targeting of iRGD peptide, SAIP@NPs exhibited strong binding to integrin $\alpha v\beta 3$, which was highly expressed on the membrane of MDA-MB-231 cells, improving the uptake capacity of tumor cells, inhibiting the rapid growth of tumor cells, and promoting tumor cell apoptosis. The results of animal experiments further proved that SAIP@NPs had longer residence time in tumor sites, stronger anti-tumor effect, and no obvious toxicity to major organs of experimental animals.

Conclusion: The engineered SAIP@NPs exhibited superior functionalities including efficient membrane permeability, precise tumor targeting, and imaging, thereby significantly augmenting the therapeutic efficacy against breast cancer with a favorable safety profile.

Keywords: silicon dioxide nanoparticles, gold nanoclusters, iRGD penetrating peptide, integrin $\alpha v\beta 3$, tumor targeting, breast cancer

Introduction

Breast cancer (BC) is a major focus of global health attention due to its high rates of occurrence and death in women with cancer.[1] Among new cancers in women, BC accounts for about 24.5% of overall cancer incidence and 15% of mortality, affecting about 2.26 million women worldwide each year, and roughly 685,000 individuals succumb to the illness.[2] In China, there has been a rapid increase in the occurrence of BC in the past few years, and the number of initial cases and deaths each year have reached 420,000 and 130,000, respectively,[3] posing a grave peril to human health and the

Graphical Abstract
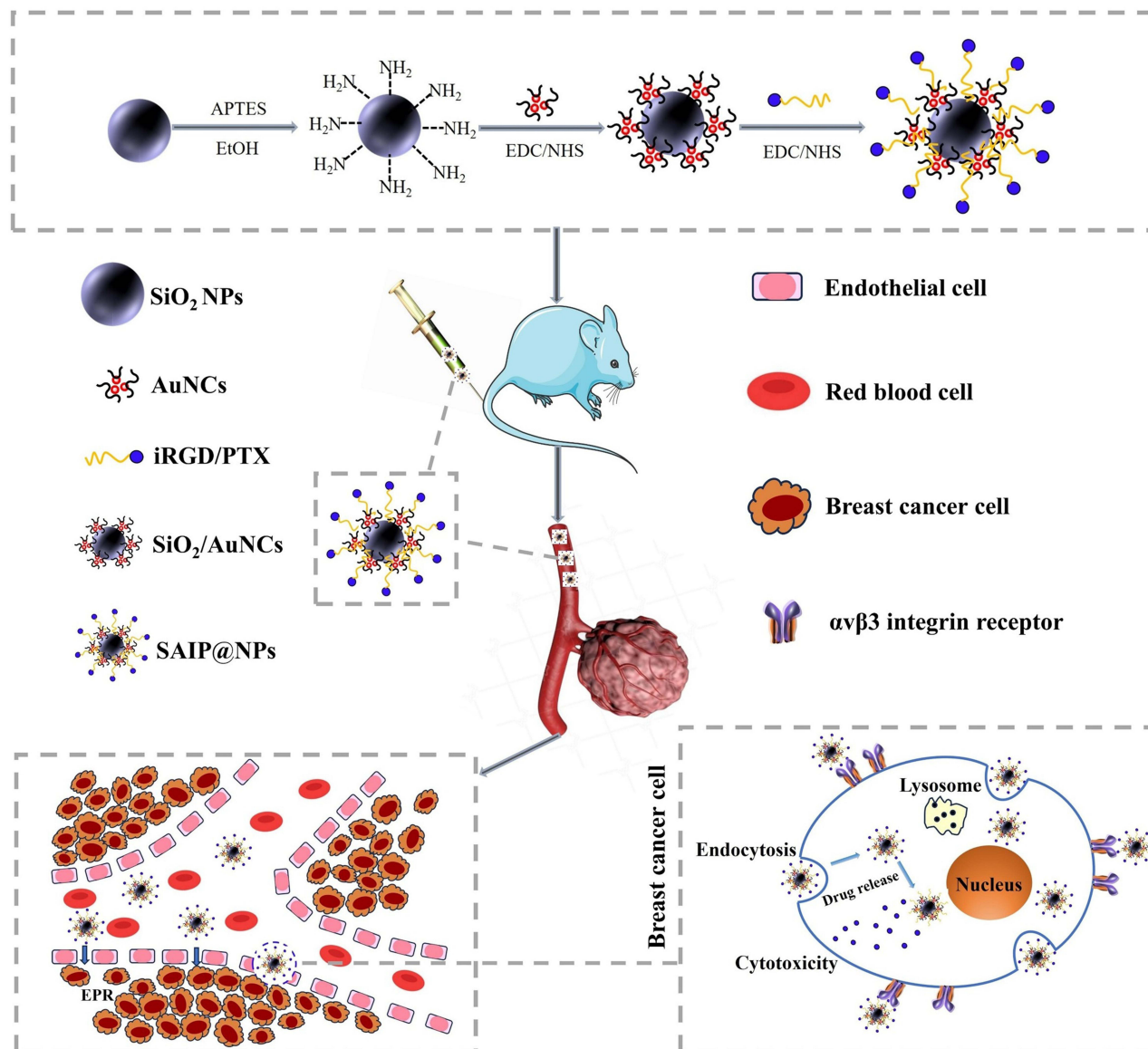
sustainability of our species. Hence, there is an immediate need to investigate additional treatment methods and strategies that are both safe and efficient in addressing the current state of BC.

At present, primary treatment for breast cancer involves predominantly surgical intervention in the early stage and chemotherapy in the late stage.[4] Although chemotherapy drugs can kill rapidly growing tumor cells, they have strong toxic side effects on the body owing to their lack of selectivity.[5–7] In addition, the water solubility of some chemotherapy drugs is very poor, which will also bring greater difficulties to the preparation and its absorption in the body.[8] Secondly, the antibody-drug directly binding complex has high targeting efficiency and little damage to normal tissues.[9–11] However, as a result of the substantial molecular weight of the antibody, it is difficult to cross the biofilm, resulting in low efficiency of penetration into tumor tissues, and easy to lose activity in the process of binding with drugs. Therefore, how to make drugs exert better anti-tumor effects and how to optimize the drug's penetration and distribution within the

lesion tissue, while mitigating its systemic toxicity, have become acute problems necessitating resolution in clinical treatment.

The development of nano-scale drug delivery systems offers a potential solution to address the constraints associated with the use of chemotherapy medications.[12,13] Nano-delivery systems are made of natural or synthetic polymer materials in which the drug is wrapped inside or modified on its surface, relying on the physicochemical properties to achieve passive targeted drug delivery. Compared with traditional dosage forms, nano-drug delivery systems show significant advantages,[14,15] such as enhancing the ability of hydrophobic medications to dissolve and remain stable, altering their distribution in the body, and regulating the rate at which they are released. In addition, the construction of a multifunctional delivery system can realize the integration of tumor imaging as well as targeted radiotherapy, chemotherapy, hyperthermia, and so on. Further, after nanoparticles are modified with specific antibodies, ligands, folic acid, hyaluronic acid, polypeptides, and other special substances, they are more likely to bind to biomolecules in target cells, thus achieving active targeting function.[16–18]

RGD peptide is a kind of short peptide containing the structure of arginine-glycine-aspartic acid, which is widely found in organisms.[19] It is the binding site of various extracellular ligand proteins and integrins and plays a pivotal role in facilitating the attachment of cancerous cells to the matrix outside of the cells.[20,21] Among them, iRGD (CRGDK/RGPD/EC) is a cyclic peptide with both RGD sequence and C-terminal sequence (Cend R), which is involved in the activation of multiple signal transduction pathways, attaching to the receptors of integrin $\alpha v\beta 3$ and $\alpha v\beta 5$ that are abundantly present on the exterior of cancerous cells, and exposing the Cend R fragment through hydrolysis.[22–24] The Cend R fragment can target Neuropilin-1 (NRP-1) on the cell surface to activate cellular endocytosis and improve vascular permeability.[25] iRGD possesses both RGD sequence and C-terminal sequence and has dual functions of targeting and membrane penetration.[26,27] Its targeting depends on its binding with integrin, and its change in cell permeability depends on its binding with NRP-1. Based on the above properties, iRGD-modified nanocarriers have the potential to potentiate the ability of drugs to selectively target tumor vascular endothelial cells and penetrate tumor new microvessels, thereby increasing drug concentration in tumor tissues.[28] Moreover, recent studies have shown that iRGD itself can inhibit tumor metastasis, which can also achieve the purpose of inhibiting tumor metastasis while improving the targeting efficiency of the drug delivery system.[29,30]

In the previous research process, we prepared silicon dioxide nanoparticles (SiO$_2$NPs) with uniform particle size and decorated their surfaces with gold nanoclusters (AuNCs) that emit red fluorescence to prepare SiO$_2$/AuNCs.[31] The antibody was then modified on SiO$_2$/AuNCs to act as a fluorescent immunosensor probe to detect tumor markers in the patient's serum. The probe had uniform particle size, good dispersion in water, good biocompatibility, large surface area, and can emit red fluorescence, which was convenient for cell imaging in vitro, and can be considered as a carrier of anti-tumor drugs. However, if it was to be used in anti-tumor aspects, it was necessary to solve the problems of membrane penetration and targeting of the carrier. Through the literature review, we learned that iRGD had dual functions of membrane penetration and targeting. Therefore, we believed that iRGD can be covalently bound to the anti-tumor drug paclitaxel (PTX) and then modified on the surface of SiO$_2$/AuNCs to construct an iRGD-targeted nano drug delivery system. Thus, breast cancer was chosen to be a tumor model to investigate the anti-tumor effects of the targeted drug delivery system at the cellular and overall animal levels.

The drug delivery system had the capability to augment the aqueous solubility of PTX, as well as address the issues related to poor targeting efficiency and limited drug loading commonly associated with traditional targeting agents. Moreover, the drug delivery system also had an imaging function, which was convenient to monitor, diagnose, and judge the progress of tumors and the anti-tumor effect of drugs, and can provide a good idea and method for tumor diagnosis and adjuvant treatment.

Materials and Methods
Materials

PTX (99%) was purchased from Solarbio Science & Technology Co., Ltd (Beijing, China). Tetraethoxysilane (TEOS), 3-Aminopropyltriethoxysilane (APTES), Chloroauric acid (HAuCl$_4$·4H$_2$O), Bovine serum albumin (BSA), 1-Ethyl-3-(3-dimethylaminopropyl) carbodiimide hydrochloride (EDC), N-hydroxysuccinimide (NHS), 6-Maleimidohexanoic acid

(MCA), Dimethyl sulfoxide (DMSO), (3-Dimethylaminopropyl) ethyl-carbodiimide monohydrochloride (EDCI), Tween 80 was purchased from Aladdin Chemistry Co., Ltd (Shanghai, China). MDA-MB-231 cells were supplied by Wuhan Service Biotechnology Co., Ltd. (Wuhan, China). All remaining chemicals were either of analytical grade or chromatographic grade and were utilized in their original state. iRGD (90%) was customized by China Peptides Co., Ltd (Shanghai, China).

Animals

Balb/c-nude mice (♀, 18~20 g) were obtained from Henan SCBS Biotechnology Co., Ltd (License number: SCXK (Yu) 2020–0005) and were raised in the SPF Animal Laboratory Center of Wannan Medical College. All the nude mice ate and drank freely and were reared at (23±2) °C and relative humidity (55±10) % for one week before the experiment.

Preparation of SiO$_2$/AuNCs

SiO$_2$NPs were prepared with a slight modification according to our previous work.[32] 90 mL 95% ethanol, 2.7 mL 28% ammonia solution, and 5 mL distilled water were successively added to the treated beaker. About 2.7 mL TEOS was added to the solution. After sonication for 10 min, the resultant blend was stirred at ambient temperature for 24 h. Subsequently, 0.4 mL of APTES was introduced into the blend and stirred consistently for a duration of 6 h. The suspension was subjected to three ethanol washes and dried to obtain the amino-functionalized silicon dioxide nanoparticles (NH$_2$-SiO$_2$NPs). Twenty-milligram NH$_2$-SiO$_2$NPs were ultrasonically dispersed in 2.0 mL of AuNCs colloidal solution. About 0.6 mg NHS and EDC were added and activated for 30 min. The solution was subjected to magnetic stirring for 12 h and washed three times to obtain SiO$_2$/AuNCs.[31]

Preparation of iRGD/PTX

Preparation of iRGD/PTX was divided into two steps, and MCA-PTX needed to be prepared first.[33] Simply, PTX (20 mg, 0.023 mmoL) and MCA (50 mg, 0.23 mmoL) were dissolved in 2 mL of DMSO. Then, EDCI (70 mg, 0.37 mmoL) was added to the solution and stirred at room temperature for 96 h before vacuum evaporation. Next, iRGD (4 mg) was dissolved in DMSO (1 mL). MCA-PTX (20 mg) was added and stirred at room temperature for 48 h. The mixture was then added to 10 mL of deionized water under ultrasound. The resulting mixture underwent dialysis using deionized water for a period of 3 days (MWCO: 3500 Da). Following centrifugation, the liquid on top was collected and subjected to lyophilization. The structure of the prepared iRGD/PTX was verified through ^{1}HNMR (AVANCE III 600M, Bruker, Germany).

Preparation SiO$_2$/AuNCs-iRGD/PTX (SAIP@NPs)

Twenty-milligram SiO$_2$/AuNCs were ultrasonically dispersed in 10 mL distilled water, and 10 mg iRGD/PTX was added for a further ultrasound for 5 min. The addition of a suitable quantity of EDC and NHS was followed by 30 min of activation through magnetic stirring. The mixture underwent continuous stirring for a period of 24 h and was subsequently rinsed with water on three occasions. After freeze-drying, SiO$_2$/AuNCs-iRGD/PTX (SAIP@NPs) was obtained. The nano-drug delivery system was characterized by fluorescence spectrum (Cary Eclipse, Agilent, USA) and TEM (JEM1200EX, JEOL, Japan). The particle size distribution and zeta potential of the nano-drug delivery system were measured with a nanoparticle particle size analyzer (Litesizer 500, Anton Paar, Austria).

Drug Loading (DL) and Encapsulation Efficiency (EE)

The centrifugation of the mixture was carried out at 10,625 g for a duration of 10 min. The resulting supernatant underwent filtration through a 0.22 μm microporous filter membrane and was later analyzed using a high-performance liquid chromatography (HPLC) system equipped with a C18 column set at 227 nm (LC-20A, Shimadzu, Japan). This trial was carried out three times to guarantee the consistency of results. The column was thermostatted at 30 °C, and a 10 μL sample injection volume was employed and a mobile phase consisting of methanol-acetonitrile-deionized water (40:30:30, vol/vol/vol), flowing at a rate of 1 mL/min. The percentages of drug loading (DL %) and encapsulation efficiency (EE %) for SAIP@NPs were computed based on the following formula.

$$DL\ (\%)= \text{Amount of PTX encapsulated}/\text{Amount of SAIP@NPs} \times 100\%$$

$$EE\ (\%)= \text{Amount of PTX encapsulated}/\text{Amount of PTX added} \times 100\%$$

Release of SAIP@NPs in vitro

The PTX release profile from SAIP@NPs was investigated using dialysis in PBS buffers under pH 5.6 and pH 7.4 conditions (10 mmoL, 0.5% Tween 80), respectively.[33] Twenty-milligram SAIP@NPs were put in a dialysis tube (MWCO: 8000–14000 Da). The stationary dialysis tube was submerged in 40 mL of the release medium and agitated at 37 °C with a speed of 100 rpm. At 0, 0.25, 0.5, 1, 2, 4, 8, 12, 24, 36, 48, and 72 h, 1 mL of the release medium was aspirated and replenished with 1 mL of fresh medium. The PTX concentration in the solution was quantified using HPLC as detailed earlier. The PTX release rate was computed using the following formula.

$$\text{Cumulative release rate}\ (\%)= \text{cumulative drug release}/\text{total drug dose} \times 100\%$$

Cytotoxicity Against MDA-MB-231 Cells

Cells from the MDA-MB-231 line in the logarithmic growth phase were plated onto 96-well plates at a density of 5×10^3 cells/well in DMEM supplemented with 10% FBS.[34] After 24 h of incubation in 5% CO_2 at 37 °C, the supernatant was removed and 100 μL-free iRGD, free PTX, free iRGD + free PTX, and SAIP@NPs with three different concentrations were added and cultivated in an incubator. After waiting 24 h, the cell condition was investigated employing the microscope. Following this, 10 μL of a 5 mg/mL MTT solution was dispensed into each well and incubated for an additional 4 h. Upon removal of the supernatant, 100 μL of DMSO was added to solubilize the formazan crystals. The absorbance at 490 nm was then measured using a microplate reader (Epoch, BioTek, USA), and cell viability (%) was subsequently calculated using the following formula.

$$\text{Cell viability}\ (\%)= \left(A_{sample}-A_{blank}\right)/\left(A_{control}-A_{blank}\right) \times 100\%$$

Cell Apoptosis Test

Flow cytometry (FCM) was employed to evaluate the cellular apoptosis rate.[35] MDA-MB-231 cells were plated onto 6-well dishes at a density of 4×10^5 cells/well. Following exposure to free PTX, SiO_2/AuNCs, and SAIP@NPs (40 μg/mL as PTX) for 24 h, the culture medium was aspirated and rinsed with PBS. Then, the handled cells were digested with trypsin without EDTA for 15 min. The cells were harvested by centrifugation and rinsed with PBS buffer (with 1% BSA). Then, according to the instructions provided in the kit, they were labeled with annexin V-FITC for 25 min and PI for 5 min. Subsequently, the cells obtained were combined with 0.5 mL of PBS buffer and transferred into a flow tube. The apoptosis was measured by flow cytometry (FACSVerse, BD, USA).

Cellular Uptake

The MDA-MB-231 cells with good logarithmic growth were selected as experimental cells and removed the nutrient solution from the surface of the cells and rushed twice with PBS (0.01moL, pH 7.4). After that, the digested cells are collected in a test tube. About 0.1 mL cell suspension and 0.9 mL DMEM were, respectively, added into three confocal cell culture dishes at a density of 4×10^5 cells/dish. After repeated blowing several times to make the cells evenly distributed, 0.5 mL of AuNCs, SiO_2/AuNCs, and SAIP@NPs were added and incubated for 2 h, respectively. Each dish was subjected to three rounds of PBS washing, followed by fixation of the cells with 4% paraformaldehyde for 15 min. Subsequently, the cell nuclei were stained with Hoechst 33342 dye (10 μg/mL) for 10 min, washed twice with PBS, and then an appropriate volume of PBS was added to each dish. Cell uptake and intracellular distribution were observed by laser confocal microscopy (TCS-SP8, Leica, Germany) in 405 nm and 633 nm laser excitation samples and photographed under a 63-x oil lens.[36]

Tumor Targeting Study in vivo

The balb/c-nude mice xenografted with MDA-MB-231 tumors, each with a volume of up to 500 mm^3, were divided into three groups of three mice each in a random manner. The free Cy7, Cy7-SiO$_2$/AuNCs-and Cy7-SAIP@NPs were intravenously injected into each group. At 1, 2, 4, 8, 12, and 24 h, the mice were anesthetized by inhalation with 2% isoflurane. The small animal imaging system (Lumina LT Series III, PerkinElmer, USA) was used to capture the fluorescence images.[37]

Tumor Model Construction

MDA-MB-231 with a good growth state was selected, suspended into 1×10^7 cells/mL with PBS, and then mixed with the basement membrane matrix in equal volume. An insulin syringe was used to inject 0.2 mL subcutaneously into the fat pad of the right breast of female balb/c-nude mice. The inoculated mice were carefully fed and the tumor growth was recorded several times.

Antitumor Effect Study in vivo

When the mean tumor volume of the mice reached 100 mm^3, the mice were stratified into four cohorts: control group, free PTX (10 mg/kg), low dose (5 mg/kg), and high dose (10 mg/kg) of SAIP@NPs, with 5 mice in each group. Each treatment group was injected with the corresponding drug through the tail vein every 2 days for two weeks. The control group received an equivalent amount of saline solution. The mice's weight and tumor size were documented. After 14 days, the mice in both groups were humanely euthanized. Stripping the tumor and weighing, and by the following formula to compute the tumor inhibition rate (%).

$$\text{Tumor inhibition rate}(\%) = (1 - W_{\text{test}}/W_{\text{control}}) \times 100\%$$

Where, W_{test} and W_{control} are the average tumor weight of the control group and tested groups.

The vital organs, including the myocardium, hepatic tissue, splenic tissue, pulmonary tissue, and renal tissue were procured for the purpose of evaluating the main visceral toxic effects of drug delivery system.

Statistical Analysis of Data

The experimental data were analyzed using SPSS 21.0 and expressed as the means ±SD. A paired *t*-test was employed to assess the statistical significance of differences between two sets of data, and *p*-value <0.05 indicated a significant difference.

Results and Discussion
^{1}H NMR Spectra of MCA-PTX and iRGD/PTX

Before the preparation of iRGD/PTX, MCA was esterified with PTX to produce MCA-PTX. Then, iRGD was conjugated with MCA-PTX through a Michael addition reaction involving sulfhydryl groups (-SH) to form iRGD/PTX.[33] It can be observed from Figure 1A, the ^{1}H NMR spectra of MCA-PTX showed the characteristic signals of MCA at δH (ppm) 7.00 (32), 3.21 (31), 2.29 (27), 1.52 (30), 1.36 (28), and 1.18 (29). In the ^{1}H NMR spectrum of iRGD/PTX (Figure 1B), the absence of the maleimide characteristic signal at δH (ppm) 7.00 indicates successful conjugation of iRGD with MCA-PTX, signifying the completion of the coupling reaction.

Characterization of SAIP@NPs

SAIP@NPs was prepared by a two-step method. First, AuNCs that emit red fluorescence were fixed onto NH$_2$-SiO$_2$NPs' surface through an amide reaction in order to obtain SiO$_2$/AuNCs. Next, with the help of EDC and NHS, the amino groups (from SiO$_2$/AuNCs) and carboxyl groups (from iRGD-PTX) were reacted by amide reaction again to obtain SAIP@NPs.

The BSA-protected AuNCs were synthesized according to the reference.[38] The prepared Au NCs had the double protection of Au-S bond and BSA steric hindrance, so that it can maintain good stability under various conditions, such
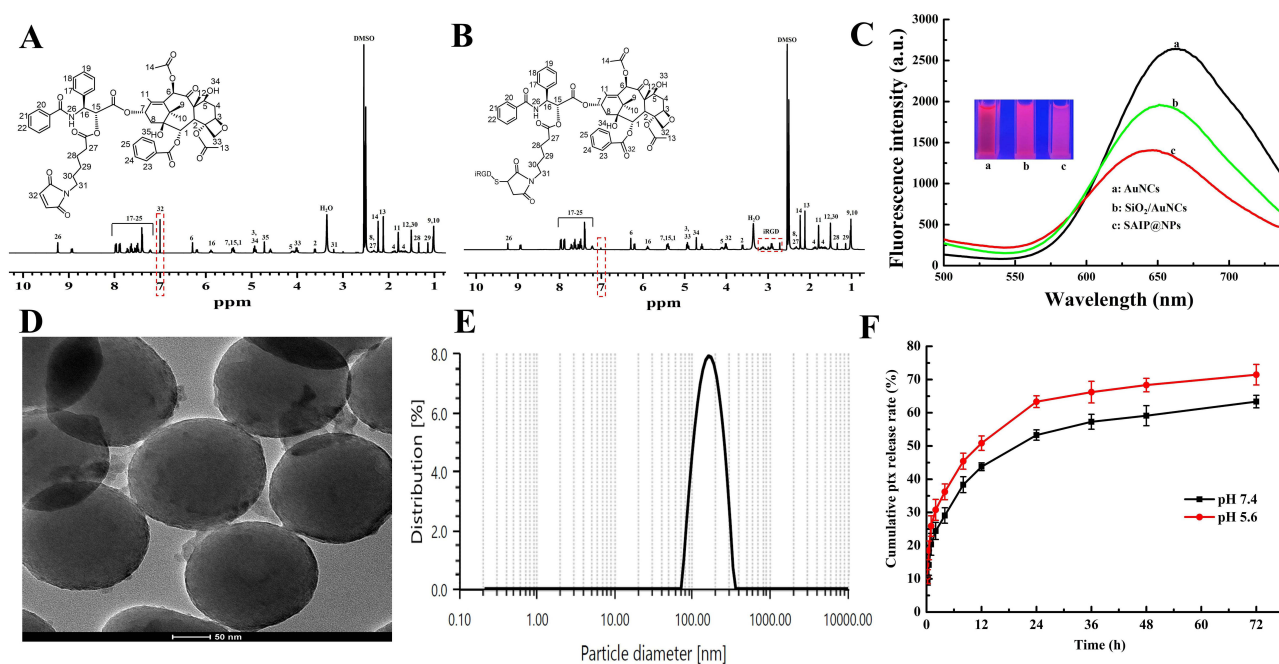
Figure 1 Characterization of SAIP@NPs. (**A**) ^{1}H NMR spectra of MCA-PTX in DMSO-D$_6$, (**B**) ^{1}H NMR spectra iRGD/PTX in DMSO-D$_6$, (**C**) fluorescence spectra, (**D**) TEM image, (**E**) size distribution and (**F**) in vitro PTX release curves of SAIP@NPs.

as different pH values, high salt, and different types of buffering systems. Under the excitation of 380 nm, AuNCs emitted a fluorescence signal peak at 660 nm, which appeared deep red under ultraviolet irradiation.

SiO$_2$NPs can maintain good strength, toughness and stability under high temperature and different chemical environments. Amino or carboxylated silica nanoparticles can further modify enzymes, proteins, DNA molecules on their surface through amidation reactions to meet their biological applications.[39] When AuNCs were decorated on the surface of NH$_2$-SiO$_2$NPs to form SiO$_2$/AuNCs, they can still maintain good stability at different pH values.

Compared with AuNCs, the fluorescence peak positions of SiO$_2$/AuNCs and SAIP@NPs were slightly blue-shifted, and their fluorescence intensity gradually decreased due to a series of preparation operations (Figure 1C). The blue shift might be caused by the change in pH value or charge during the experiment.[40] TEM imaging in Figure 1D and particle size distribution in Figure 1E revealed that the morphology of SAIP@NPs was a consistent round form with a relatively uniform particle size distribution of about 160 nm. The zeta potentials of NH$_2$-SiO$_2$, AuNCs, SiO$_2$/AuNCs, and SAIP@NPs in deionized water were +0.6, −18.1, −31.2, and −9.5, respectively. It is inferred that the negative charges at the exterior of the drug delivery system came from AuNCs. The hydrodynamic size and presence of a negative surface charge on SAIP@NPs allowed the NPs to evade non-specific uptake by cells and instead accumulate specifically at the site of the tumor.[41,42]

Determination DL and EE

The data detected by HPLC were substituted into the PTX standard curve equation established in advance to acquire DL and EE of SAIP@NPs were 23.17%±0.14% and 90.26±1.16%, respectively. In general, the DL of traditional nanoparticles was not greater than 10%.[43,44] SAIP@NPs which exhibited a high PTX loading capacity may be mainly attributed to the following two aspects: (1) SiO$_2$ NPs were a typical inorganic nanomaterial with good adsorption performance. During the construction of the drug delivery system, part of PTX was covalently bound by amide bonds, while the other part of PTX can be loaded onto the surface of SiO$_2$/AuNCs by physical adsorption; (2) The prepared AuNCs (about 5 nm) were loaded onto the silicon spheres to form composite nanoparticles, which further increased the specific surface area of the carrier, resulting in the improvement of PTX loading capacity, underscoring their significant potential for application in anti-cancer therapy.

In vitro Release

The in vitro release of SAIP@NPs was investigated in PBS buffers at pH 5.6 and pH 7.4. As can be seen from Figure 1F, PTX release from SAIP@NPs was more ideal in the pH 5.6 PBS buffer, which was due to the fact that under acidic conditions, the ester bond connecting the linker and PTX in the drug delivery system was more prone to hydrolytic fracture.[45] In the range of 0.25–72 h, the drug delivery system exhibited a sustained PTX release behavior, and the cumulative release amount of PTX after 72 h at pH 5.6 and pH 7.4 PBS buffer was 71.45% and 63.36%, respectively. The acidic microenvironment of tumor tissue is conducive to the breakage of amide bonds in SAIP@NPs. This may result in easier release of PTX from SAIP@NPs under slightly acidic conditions.

In vitro Cytotoxicity

To investigate the cytotoxicity of the nanocarriers on tumor cells, an MTT assay was adopted to detect the survival rate of cells treated with MDA-MB-231 by free iRGD, free PTX, free iRGD + free PTX, and SAIP@NPs. After treatment for 24 h, there was no cytotoxicity to MDA-MB-231 cells even if the concentration of free iRGD was as high as 200 μg/mL, while the cytotoxicity was small when the concentration of free PTX was lower than 20 μg/mL, and gradually enhanced when the concentration was higher than 20 μg/mL (Figure 2A). This was attributed to the lower cytotoxicity profile of PTX compared to other chemotherapeutic agents, necessitating relatively high doses for therapeutic efficacy.[46] Therefore, combined with the above experimental conditions, we chose a PTX concentration of 40 μg/mL for follow-up experiments. Compared with free PTX, free PTX + free iRGD exhibited almost the same cytotoxicity regardless of 24 h or 48 h, while SAIP@NPs showed significantly enhanced cytotoxicity (Figure 2B). This may be due to iRGD modification, enhancing the nanoparticles of MDA-MB-231 cell penetration, effectively promoting the SAIP@NPs intracellular accumulation and the
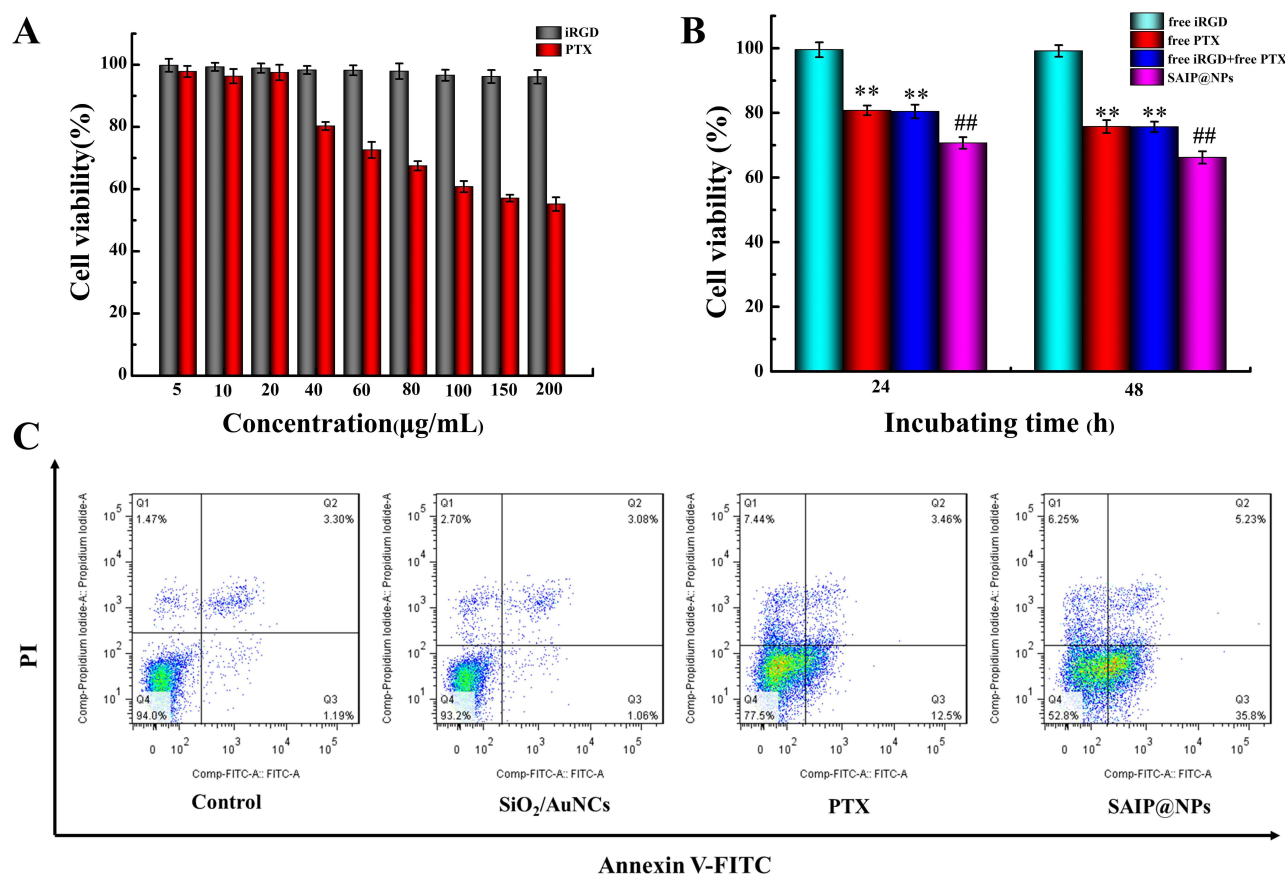

Figure 2 In vitro cell cytotoxicity and cell apoptosis against MDA-MB-231 cells. (**A**) After incubation with MDA-MB-231 cells for 24 h, the cytotoxic effects of free iRGD and free PTX at different concentrations. (**B**) Comparison of cytotoxicity of free iRGD (40 μg/mL), free PTX (40 μg/mL), free PTX (40 μg/mL) + free iRGD (40 μg/mL), SAIP@NPs (including 40 μg/mL PTX) in vitro. **$p<0.01$, vs free iRGD; ##$p<0.01$, vs free PTX. (**C**) Apoptosis detection of MDA-MB-231 cells.

intracellular release of PTX. Because the free PTX was no load on the nanoparticles, so difficult to effectively penetrate the interior of the tumor cells, its effective concentrations of intracellular are lower than SAIP@NPs group. These results suggested that the nanocarriers exhibited better in vitro antitumor activity than free PTX and also confirmed that iRGD covalently bound to PTX without reducing the effectiveness of PTX.

Cell Apoptosis

The Annexin V-FITC/PI kit was used to stain MDA-MB-231 cells in early and late stages of apoptosis, and flow cytometry was employed to determine the proportion of apoptotic cells. From Figure 2C, it was observed that SAIP@NPs showed a higher apoptosis rate (Q2 + Q3, 41.03%) after 24 h of cell treatment compared with free PTX (Q2 + Q3, 15.96%). This indicated that SAIP@NPs could promote cell uptake, accelerate PTX-induced apoptosis, and better exert the anti-tumor effect of PTX. In addition, the apoptosis rate of SiO$_2$/AuNCs group without PTX (4.14%) was not much different from that of the control group (4.49%), suggesting that the drug delivery system was relatively safe and less toxic.

Cellular Uptake

The internalization of the drug delivery system by MDA-MB-231 cells was visualized using laser confocal microscopy to assess the membrane permeation of iRGD. In Figure 3, the blue fluorescence was the nuclear position after staining with Hoechst 33342, and the red fluorescence was caused by the emission of AuNCs. Since AuNCs were synthesized under mild conditions protected by BSA and had good biocompatibility,[38] the cells survived well after co-culture with MDA-MB-231 cells for 2 h. However, due to the small size of AuNCs (about 2 nm) and the absence of targeted molecular
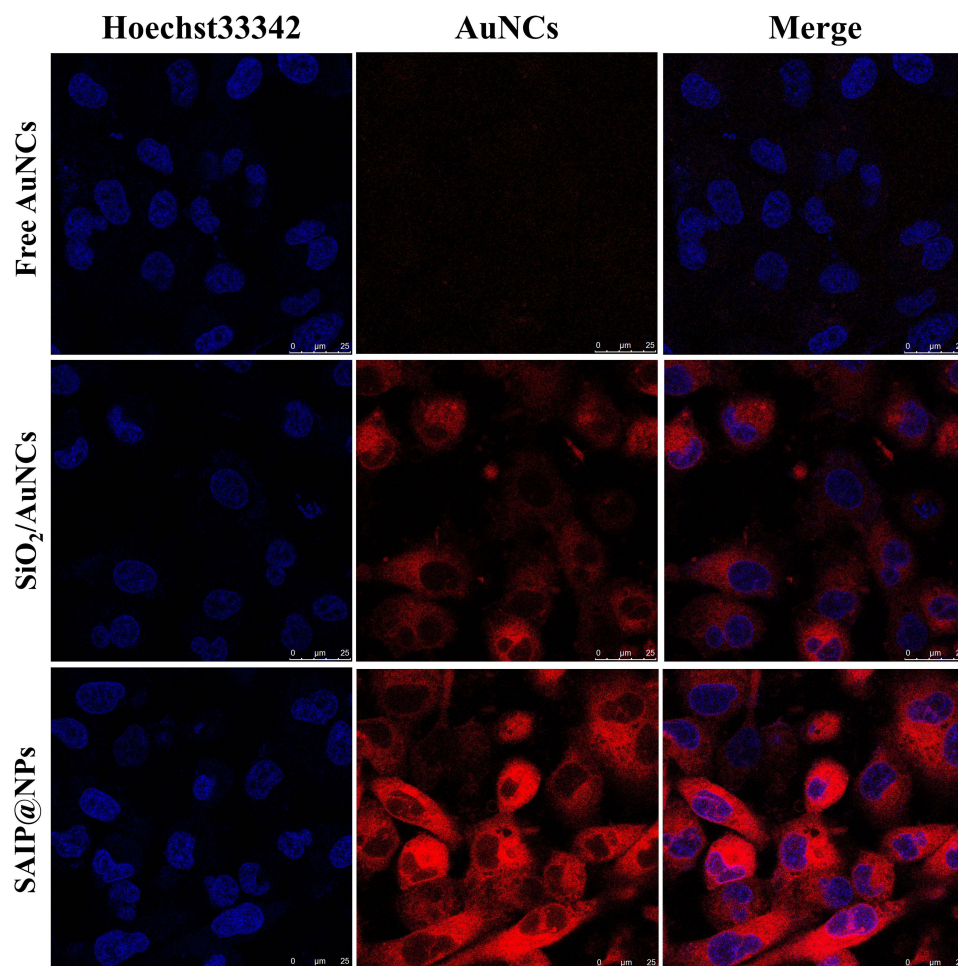

Figure 3 Uptake of nanoparticles by MDA-MB-231 cells.

modification, AuNCs were washed off during the experimental operation, and no obvious red fluorescence was observed in tumor cells. At the same time, the size of the SiO_2/AuNCs was about 140 nm, and although there was no iRGD modification, the nano complex themselves had a good affinity for cells and were able to exert a certain passive targeting effect, so weak red light can be observed around the breast cancer nucleus. SAIP@NPs not only had the function of membrane permeability but also had the targeting function and demonstrated a high affinity for the integrin αvβ3,[47] which is overexpressed in tumor tissues; therefore, a strong fluorescence signal can be observed in tumor cells.

In vivo Biodistribution

To investigate the biological distribution of the drug delivery system in animals, near-infrared fluorescent pigment Cy7 was used to label the nanoparticles.[48] Free Cy7, Cy7-SiO_2/AuNCs, Cy7-SAIP@NPs were injected intravenously into MDA-MB-231 tumor-bearing nude mice for observation through the animal imaging system, and the results are shown in Figure 4. After intravenous injection of free Cy7, the fluorescent signal was almost undetectable at the tumor site, which may be attributed to the fact that free Cy7 in the bloodstream was rapidly hepatic uptake and subsequent excretion result in limited tumor bioaccumulation. However, the accumulation of Cy7-SiO_2/AuNCs and Cy7-SAIP@NPs at the tumor site was rapid following injection, reaching its peak within 2–4 h. After 4 h, Cy7-SiO_2/AuNCs gradually left the tumor site, and the fluorescence signal gradually attenuated with clearance. In the meantime, strong fluorescence was still observed in the Cy7-SAIP@NPs group at 8 h, and then gradually cleared by the body. This may be due to the gradual capture of Cy7-SAIP@NPs by the liver, allowing it to accumulate at the tumor site over a long period of time through EPR effects and the interactions of iRGD with integrin αvβ3, which is upregulated on the endothelial cells within tumor microvasculature.[49]
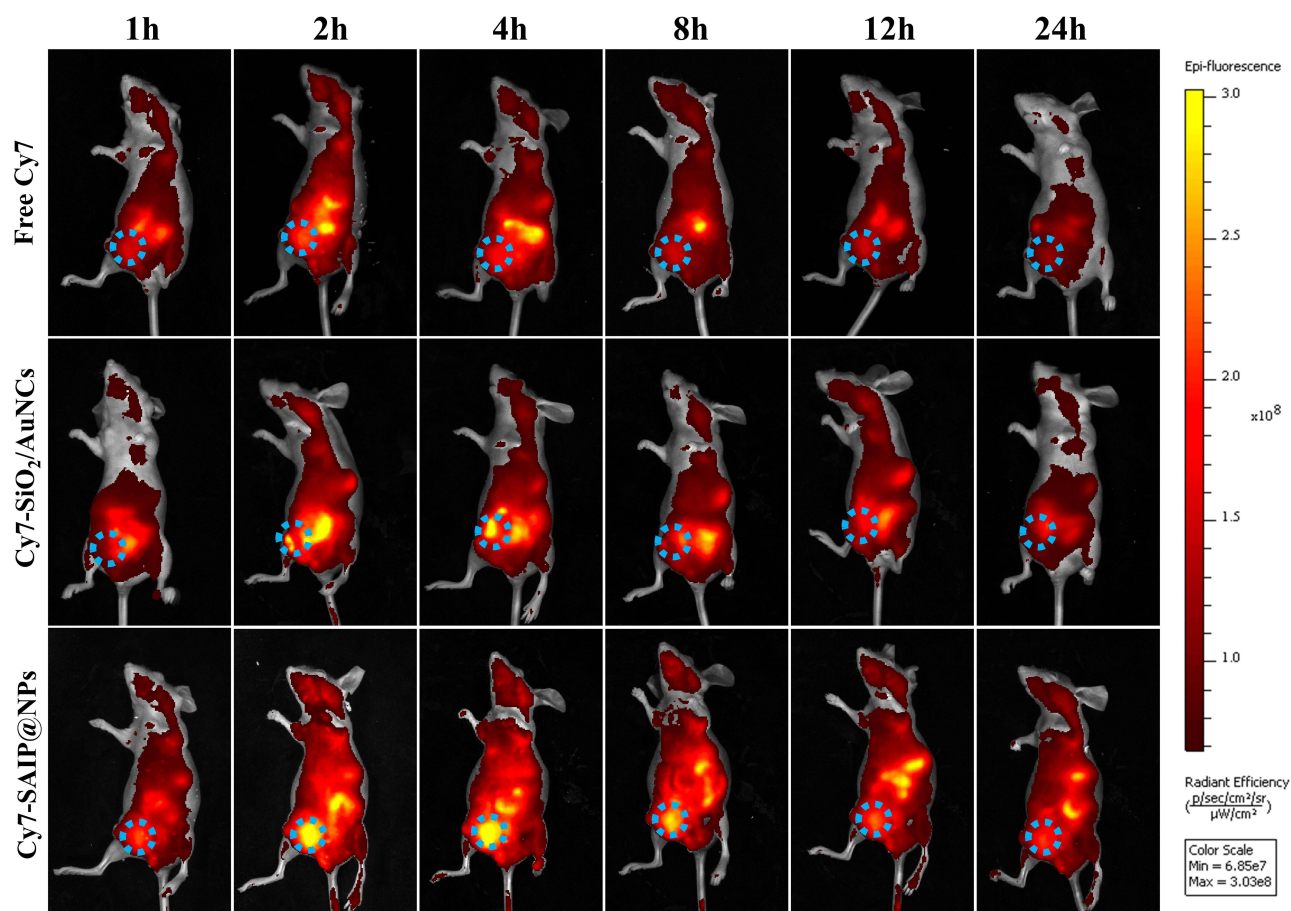

Figure 4 In vivo tumor targeting of Cy7-SAIP@NPs.

Antitumor Effect Study in vivo

Normal saline, free PTX, low-dose, and high-dose of SAIP@NPs were injected into MBD-MB-231 tumor-bearing mice via tail vein, respectively, and the weight changes and tumor growth of each group were recorded.

As shown in Figure 5A, the body weight of mice in the control group had been in a state of continuous growth because the injection of normal saline had no inhibitory effect on tumor growth, while the body weight growth rate of mice in other groups (including the drug-carrying system group) was significantly lower than that of the control group.

The alterations in tumor volume within each cohort are illustrated in Figure 5B. Within the 14-day treatment period, the tumor growth of mice in the control group was rapid because they were not inhibited by the drug. Compared with the control group, the tumor volume of the other groups showed an overall upward trend, but the growth rate was slower. In comparison to the control group, a significant statistical variance was observed in the PTX group and the low-dose SAIP@NPs group ($p<0.05$), and a substantial and statistically significant variance was observed in the high-dose SAIP@NPs group ($p<0.01$).

Upon completion of the therapy, the mice in each group were euthanized, tumor-stripped, and weighed, and the results are shown in Figure 5C and D. Relative to the control group, the tumor weight of mice in the drug-loading system group was significantly decreased ($p<0.05$, $p<0.01$). The tumor inhibition effect of the high-dose SAIP@NPs group (60.83%) was better than that of low-dose SAIP@NPs group (55.04%) and PTX group (37.52%). The results showed that the drug delivery system can play a good anti-tumor effect by inducing apoptosis and inhibiting tumor cell regeneration. In recent years, there are still a lot of PTX delivery systems research has shown that the inhibition rate
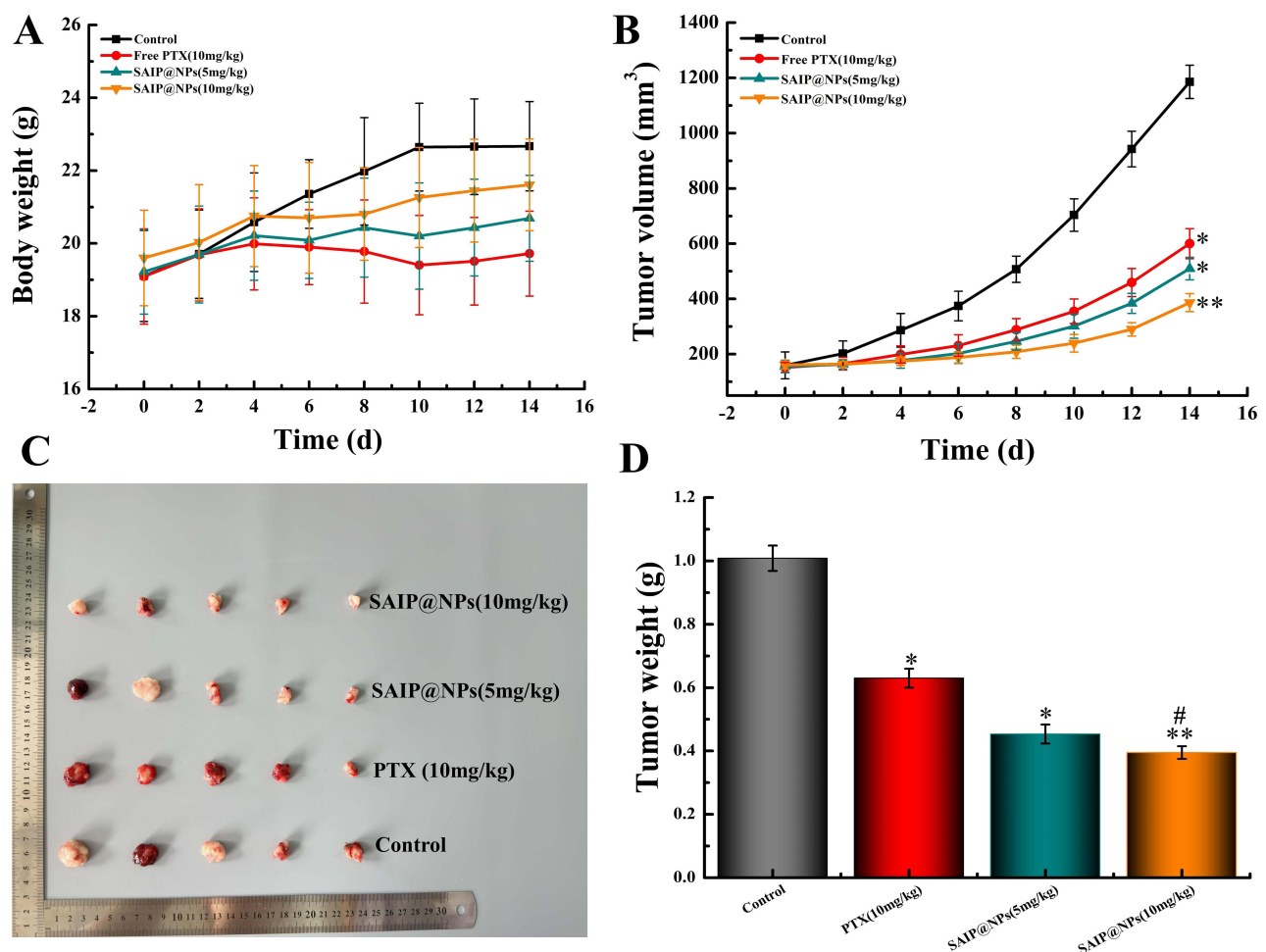

Figure 5 Antitumor effect of drug delivery system in vivo. Data were expressed as means ± SD (n = 5). (**A**) Body weight curves of mice, (**B**) tumor growth curves of mice, (**C**) tumor photos of mice, (**D**) tumor weight of mice. *p <0.05, **p <0.01 vs control, #p <0.05 vs PTX.
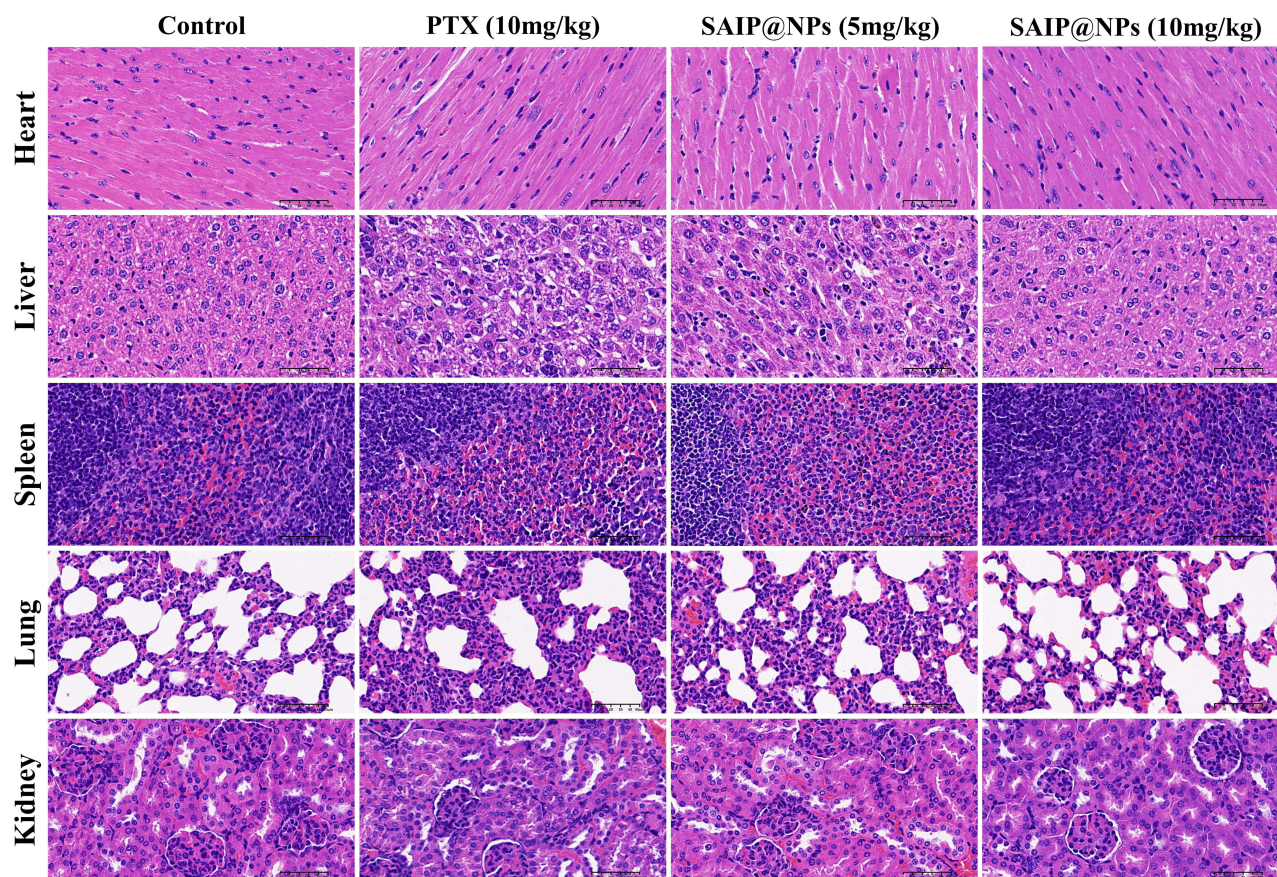
Figure 6 Histological inspection of heart, liver, spleen, lung, and kidney of MBD-MB-231 tumor-bearing mice after 14 days of intervention with different treatment strategies.

of 40–70% of breast cancer.[50–52] This implied that SAIP@NPs exhibit potential anti-breast cancer research value. However, compared with some reports of PTX drug delivery system, our current work still needs to be further explored, and the research on the anti-breast cancer mechanism of PTX needs to be further explored.

In vivo Safety Evaluation

Safety checks were very important for drug administration in injectable drug delivery systems.[53] Histological observations of the main organs in tumor-bearing mice groups, such as heart, liver, spleen, lung, and kidney, were conducted using H&E staining. The findings are presented in Figure 6. Relative to the control group, the major organs of the treatment group had no obvious pathological damage, suggesting that the constructed drug delivery system was safe and had low toxicity to the major organs of mice, which was a relatively safe injection drug delivery strategy.

Conclusion

In this study, we covalently combined iRGD and PTX, and then modified them on $SiO_2/AuNCs$ composite nanoparticles to construct an active targeted drug delivery system. SAIP@NPs showed a good sustained release effect, which has the potential to enhance the uptake capacity of MDA-MB-231 cells, suppress the proliferation of MDA-MB-231 cells, induce apoptosis in tumor cells, and increase the effectiveness of tumor site targeting, and show excellent anti-tumor effect. This drug delivery system has the capability to overcome the challenge of PTX's poor aqueous solubility but also overcome the problems of small drug loading and easy aggregation of anti-tumor drugs modified by antibodies. The system also has the functions of permeating membrane, targeting and imaging, which can provide a good idea and method for the diagnosis and adjuvant therapy of tumors.

Abbreviations

PTX, Paclitaxel; SiO_2NPs, Silicon dioxide nanoparticles; AuNCs, Gold nanoclusters; iRGD, Internalizing cyclic Arg-Gly-Asp; BC, Breast cancer; Cend R, C-terminal sequence; NRP-1, Neuropilin-1; TEOS, Tetraethoxysilane; APTES, 3-Aminopropyltriethoxysilane; $HAuCl_4 \cdot 4H_2O$, Chloroauric acid; BSA, Bovine serum albumin; EDC, 1-Ethyl-3-(3-dimethyla-minopropyl) carbodiimide hydrochloride; NHS, N-Hydroxysuccinimide; MCA, 6-Maleimidohexanoic acid; DMSO, Dimethyl sulfoxide; EDCI, (3-Dimethylaminopropyl) ethyl-carbodiimide monohydrochloride; TEM, Transmission electron microscopy; EPR, Enhanced permeability and penetration; DL, Drug loading; EE, Encapsulation efficiency; HPLC, High-performance liquid chromatography; FBS, Fetal bovine serum; FCM, Flow cytometry.

Data Sharing Statement

The data for this study can be requested from the corresponding author, subject to reasonable terms and conditions.

Ethics Approval

This research was carried out in accordance with the guidelines set forth in the Declaration of Helsinki and obtained ethical approval from the committee on ethics at Wannan Medical College, ensuring adherence to ethical standards in research (LLSC-2022-048) and conducted according to the NIH Guide for the Care and Use of Laboratory Animals.

Acknowledgments

Disclosure

The authors declare no conflicts of interest in this work.

References

1. Chai J, Hu J, Wang T, Bao X, Luan J, Wang Y. A multifunctional liposome for synergistic chemotherapy with ferroptosis activation of triple-negative breast cancer. *Mol Pharm*. 2024;21(2):781–790. doi:10.1021/acs.molpharmaceut.3c00903
2. Sung H, Ferlay J, Siegel RL, et al. Global cancer statistics 2020: GLOBOCAN estimates of incidence and mortality worldwide for 36 cancers in 185 countries. *CA Cancer J Clin*. 2021;71(3):209–249. doi:10.3322/caac.21660
3. Xia C, Dong X, Li H, et al. Cancer statistics in China and United States, 2022: profiles, trends, and determinants. *Chin Med J*. 2022;135 (5):584–590. doi:10.1097/CM9.0000000000002108
4. Iacopetta D, Ceramella J, Baldino N, Sinicropi MS, Catalano A. Targeting breast cancer: an overlook on current strategies. *Int J Mol Sci*. 2023;24 (4):3643. doi:10.3390/ijms24043643
5. Zhu L, Chen Y, Wei C, et al. Anti-proliferative and pro-apoptotic effects of cinobufagin on human breast cancer MCF-7 cells and its molecular mechanism. *Nat Prod Res*. 2018;32(4):493–497. doi:10.1080/14786419.2017.1315575
6. Li L, He S, Yu L, et al. Codelivery of DOX and siRNA by folate-biotin-quaternized starch nanoparticles for promoting synergistic suppression of human lung cancer cells. *Drug Deliv*. 2019;26(1):499–508. doi:10.1080/10717544.2019.1606363
7. Elshazly EH, Zhang S, Yu LZ, Zhang Y, Ke LX, Gong RM. Hydroxychloroquine enhances anticancer effect of DOX/folate-phytosterol-carboxymethyl cellulose nanoparticles in A549 lung cancer cells. *Trop J Pharm Res*. 2020;19(2):219–225. doi:10.4314/tjpr.v19i2.1
8. Chen Y, Wang S, Hu Q, Zhou L. Self-emulsifying system co-loaded with paclitaxel and coix seed oil deeply penetrated to enhance efficacy in cervical cancer. *Curr Drug Deliv*. 2023;20(7):919–926. doi:10.2174/1567201819666220628094239
9. Huang R, Sun Y, Gao Q, Wang Q, Sun B. Trastuzumab-mediated selective delivery for platinum drug to HER2-positive breast cancer cells. *Anticancer Drugs*. 2015;26(9):957–963. doi:10.1097/CAD.0000000000000272
10. Riccardi F, Dal Bo M, Macor P, Toffoli G. A comprehensive overview on antibody-drug conjugates: from the conceptualization to cancer therapy. *Front Pharmacol*. 2023;14:1274088. doi:10.3389/fphar.2023.1274088
11. Yang T, Li W, Huang T, Zhou J. Antibody-drug conjugates for breast cancer treatment: emerging agents, targets and future directions. *Int J Mol Sci*. 2023;24(15):11903. doi:10.3390/ijms241511903
12. Etheridge ML, Campbell SA, Erdman AG, Haynes CL, Wolf SM, McCullough J. The big picture on nanomedicine: the state of investigational and approved nanomedicine products. *Nanomedicine*. 2013;9(1):1–14. doi:10.1016/j.nano.2012.05.013
13. Abhang A, Katari O, Ghadi R, Chaudhari D, Jain S. Exploring the synergistic behavior of paclitaxel and vorinostat upon co-loading in albumin nanoparticles for breast cancer management. *Drug Deliv Transl Res*. 2024;14(2):510–523. doi:10.1007/s13346-023-01415-7

14. Colby AH, Oberlies NH, Pearce CJ, Herrera VL, Colson YL, Grinstaff MW. Nanoparticle drug-delivery systems for peritoneal cancers: a case study of the design, characterization and development of the expansile nanoparticle. *Wiley Interdiscip Rev Nanomed Nanobiotechnol*. 2017;9(3). doi:10.1002/wnan.1451

15. Wang S, Zhou D, Xu Z, et al. Anti-tumor drug targets analysis: current insight and future prospect. *Curr Drug Targets*. 2019;20(11):1180–1202. doi:10.2174/1389450120666190402145325

16. Sun Y, Shi T, Zhou L, Zhou Y, Sun B, Liu X. Folate-decorated and NIR-activated nanoparticles based on platinum(IV) prodrugs for targeted therapy of ovarian cancer. *J Microencapsul*. 2017;34(7):675–686. doi:10.1080/02652048.2017.1393114

17. Li Q, Zhou Y, He W, et al. Platelet-armored nanoplatform to harmonize janus-faced IFN-γ against tumor recurrence and metastasis. *J Control Release*. 2021;338:33–45. doi:10.1016/j.jconrel.2021.08.020

18. Hong H, Zou Q, Liu Y, Wang S, Shen G, Yan X. Supramolecular nanodrugs based on covalent assembly of therapeutic peptides toward in vitro synergistic anticancer therapy. *ChemMedChem*. 2021;16(15):2381–2385. doi:10.1002/cmdc.202100236

19. Katsamakas S, Chatzisideri T, Thysiadis S, Sarli V. RGD-mediated delivery of small-molecule drugs. *Future Med Chem*. 2017;9(6):579–604. doi:10.4155/fmc-2017-0008

20. Javid H, Oryani MA, Rezagholinejad N, Esparham A, Tajaldini M, Karimi-Shahri M. RGD peptide in cancer targeting: benefits, challenges, solutions, and possible integrin-RGD interactions. *Cancer Med*. 2024;13(2):e6800. doi:10.1002/cam4.6800

21. Fu S, Xu X, Ma Y, Zhang S, Zhang S. RGD peptide-based non-viral gene delivery vectors targeting integrin $\alpha_v\beta_3$ for cancer therapy. *J Drug Target*. 2019;27(1):1–11. doi:10.1080/1061186X.2018.1455841

22. Kang S, Lee S, Park S. iRGD peptide as a tumor-penetrating enhancer for tumor-targeted drug delivery. *Polymers*. 2020;12(9):1906. doi:10.3390/polym12091906

23. Zuo H. iRGD: a promising peptide for cancer imaging and a potential therapeutic agent for various cancers. *J Oncol*. 2019;2019:9367845. doi:10.1155/2019/9367845

24. Yin H, Yang J, Zhang Q, et al. iRGD as a tumor-penetrating peptide for cancer therapy (Review). *Mol Med Rep*. 2017;15(5):2925–2930. doi:10.3892/mmr.2017.6419

25. Sugahara KN, Teesalu T, Karmali PP, et al. Tissue-penetrating delivery of compounds and nanoparticles into tumors. *Cancer Cell*. 2009;16 (6):510–520. doi:10.1016/j.ccr.2009.10.013

26. Teesalu T, Sugahara KN, Ruoslahti E. Tumor-penetrating peptides. *Front Oncol*. 2013;3:216. doi:10.3389/fonc.2013.00216

27. Thirumalai A, Girigoswami K, Pallavi P, Harini K, Gowtham P, Girigoswami A. Cancer therapy with iRGD as a tumor-penetrating peptide. *Bull Cancer*. 2023;110(12):1288–1300. doi:10.1016/j.bulcan.2023.08.009

28. Ruoslahti E. Tumor penetrating peptides for improved drug delivery. *Adv Drug Deliv Rev*. 2017;110-111:3–12. doi:10.1016/j.addr.2016.03.008

29. Sugahara KN, Braun GB, de Mendoza TH, et al. Tumor-penetrating iRGD peptide inhibits metastasis. *Mol Cancer Ther*. 2015;14(1):120–128. doi:10.1158/1535-7163.MCT-14-0366

30. Hamilton AM, Aidoudi-Ahmed S, Sharma S, et al. Nanoparticles coated with the tumor-penetrating peptide iRGD reduce experimental breast cancer metastasis in the brain. *J Mol Med*. 2015;93(9):991–1001. doi:10.1007/s00109-015-1279-x

31. Li LH, Feng DX, Zhao JQ, Guo ZL, Zhang YZ. Simultaneous fluoroimmunoassay of two tumor markers based on CdTe quantum dots and gold nanocluster coated-silica nanospheres as labels. *RSC Adv*. 2015;128(5):105992–105998. doi:10.1039/c5ra19262e

32. Li L, Zhang W, Wei Y, Yu L, Feng D. A sensitive fluorescent immunoassay for prostate specific antigen detection based on signal amplify strategy of horseradish peroxidase and silicon dioxide nanospheres. *J Anal Methods Chem*. 2022;2022:6209731. doi:10.1155/2022/6209731

33. Hu H, Wang B, Lai C, et al. iRGD-paclitaxel conjugate nanoparticles for targeted paclitaxel delivery. *Drug Dev Res*. 2019;80(8):1080–1088. doi:10.1002/ddr.21589

34. Muhammad Zohaib H, Saqlain M, Jamil H, et al. Investigating the effect of selenium nano-particles on microbial activity and cancerous cell line of MCF-7 and MDA-MB-231. *Pak J Pharm Sci*. 2023;36(4(Special)):1331–1336.

35. Wang Y, Lan Y, Wu L, Zhang S, Su Q, Yang Q. Deguelin and paclitaxel loaded PEG-PCL nano-micelles for suppressing the proliferation and inducing apoptosis of breast cancer cells. *Front Biosci*. 2024;29(2):90. doi:10.31083/j.fbl2902090

36. Viswanathan G, Hsu YH, Voon SH, et al. A comparative study of cellular uptake and subcellular localization of doxorubicin loaded in self-assemblies of amphiphilic copolymers with pendant dendron by MDA-MB-231 human breast cancer cells. *Macromol Biosci*. 2016;16 (6):882–895. doi:10.1002/mabi.201500435

37. Pradyuth KS, Salunkhe SA, Singh AK, Chitkara D, Mittal A. Belinostat loaded lipid-polymer hybrid nanoparticulate delivery system for breast cancer: improved pharmacokinetics and biodistribution in a tumor model. *J Mater Chem B*. 2023;11(45):10859–10872. doi:10.1039/d3tb01317k

38. Xie J, Zheng Y, Ying JY. Protein-directed synthesis of highly fluorescent gold nanoclusters. *J Am Chem Soc*. 2009;131(3):888–889. doi:10.1021/ja806804u

39. Hu X, Hao X, Wu Y, et al. Multifunctional hybrid silica nanoparticles for controlled doxorubicin loading and release with thermal and pH dually response. *J Mater Chem B*. 2013;1(8):1109–1118. doi:10.1039/C2TB00223J

40. Duan Q, Yang M, Zhang B, et al. Gold nanoclusters modified mesoporous silica coated gold nanorods: enhanced photothermal properties and fluorescence imaging. *J Photochem Photobiol B*. 2021;215:112111. doi:10.1016/j.jphotobiol.2020.112111

41. Steichen SD, Caldorera-Moore M, Peppas NA. A review of current nanoparticle and targeting moieties for the delivery of cancer therapeutics. *Eur J Pharm Sci*. 2013;48(3):416–427. doi:10.1016/j.ejps.2012.12.006

42. Chen Y, Zhang Z, Qian Z, Ma R, Luan M, Sun Y. Sequentially released liposomes enhance anti-liver cancer efficacy of tetrandrine and celastrol-loaded coix seed oil. *Int J Nanomed*. 2024;19:727–742. doi:10.2147/IJN.S446895

43. Oluwadamilola Miriam K, Rosemary IA, Adebimpe IW, et al. Formulation and evaluation of paclitaxel-loaded boronated chitosan/alginate nanoparticles as a mucoadhesive system for localized cervical cancer drug delivery. *J Drug Deliv Sci Technol*. 2023;87:104810. doi:10.1016/j.jddst.2023.104810

44. Liu D, Hou T, Geng C, et al. Liposomes enhance the immunological activity of polygonatum cyrtonema hua polysaccharides. *J Pharm Sci*. 2024. doi:10.1016/j.xphs.2024.01.005

45. Liu Z, Chen X, Jin Q, et al. Dual functionalized hyaluronic acid micelles loading paclitaxel for the therapy of breast cancer. *Front Bioeng Biotechnol*. 2023;11:1230585. doi:10.3389/fbioe.2023.1230585

46. Meng Z, Lv Q, Lu J, et al. Prodrug Strategies for Paclitaxel. *Int J Mol Sci*. 2016;17(5):796. doi:10.3390/ijms17050796

47. Chen B, Liu X, Li Y, et al. iRGD tumor-penetrating peptide-modified nano-delivery system based on a marine sulfated polysaccharide for enhanced anti-tumor efficiency against breast cancer. *Int J Nanomed*. 2022;17:617–633. doi:10.2147/IJN.S343902

48. Chen Y, He Q, Lu H, et al. Visualization and correlation of drug release of risperidone/clozapine microspheres in vitro and in vivo based on FRET mechanism. *Int J Pharm*. 2024;653:123885. doi:10.1016/j.ijpharm.2024.123885

49. Jin Z, Lv Y, Cao H, et al. Core-shell nanocarriers with high paclitaxel loading for passive and active targeting. *Sci Rep*. 2016;6:27559. doi:10.1038/srep27559

50. Ye J, Li R, Yang Y, et al. Comparative colloidal stability, antitumor efficacy, and immunosuppressive effect of commercial paclitaxel nanoformulations. *J Nanobiotechnology*. 2021;19(1):199. doi:10.1186/s12951-021-00946-w

51. Dang W, Xing B, Jia X, et al. Subcellular organelle-targeted nanostructured lipid carriers for the treatment of metastatic breast cancer. *Int J Nanomed*. 2023;18:3047–3068. doi:10.2147/IJN.S413680

52. Wang Q, Xu W, Li Q, et al. Coaxial electrostatic spray-based preparation of localization missile liposomes on a microfluidic chip for targeted treatment of triple-negative breast cancer. *Int J Pharm*. 2023;643:123220. doi:10.1016/j.ijpharm.2023.123220

53. Deng H, Wang Y, Zhou Y, et al. In vitro and in vivo evaluation of folic acid modified DOX-Loaded ^{32}P-nHA nanoparticles in prostate cancer therapy. *Int J Nanomed*. 2023;18:2003–2015. doi:10.2147/IJN.S403887